Fluctuation Dynamics of Block Copolymer Vesicles

P. Falus,[1,2] M. A. Borthwick,[2] and S. G. J. Mochrie[1]

[1]*Department of Physics, Yale University, New Haven, Connecticut 06511, USA*

[2]*Department of Physics, Massachusetts Institute of Technology, Cambridge, Massachusetts 02139, USA*

(Received 28 June 2004; published 12 January 2005)

X-ray photon correlation spectroscopy was used to characterize the wave-vector- and temperature-dependent dynamics of spontaneous thermal fluctuations in a vesicle (L_4) phase that occurs in a blend of a symmetric poly(styrene-ethylene/butylene-styrene) triblock copolymer with a polystyrene homopolymer. Measurements of the intermediate scattering function reveal stretched-exponential behavior versus time, with a stretching exponent slightly larger than $2/3$. The corresponding relaxation rates show an approximate q^3 dependence versus wave vector. Overall, the experimental measurements are well described by theories that treat the dynamics of independent membrane plaquettes.

DOI: 10.1103/PhysRevLett.94.016105 PACS numbers: 68.35.Ja, 61.25.Hq

The dynamics of spontaneous shape fluctuations of vesicles [1–4] and microemulsion droplets [5–13] has attracted considerable attention. In part, this is because such systems are simple models for the biological membranes that define living cells. In addition, there are elegant theoretical predictions for the relaxation rates of the various fluctuation modes and for the intermediate scattering function (ISF), observed in dynamic light- or neutron-scattering experiments [7,9,12,14,15]. Using these theories, careful studies of membrane dynamics permit the membrane elastic constants to be measured, which in turn are believed to determine the overall phase behavior. Block copolymer-homopolymer blends can also self-assemble into membranes [16], but we are unaware of any studies to date of the equilibrium dynamics of membrane undulations in polymeric systems.

Recently, we have uncovered an equilibrium vesicle phase (L_4 phase) in blends of poly(styrene-ethylene/butylene-styrene) symmetric triblock copolymer (PSEBS) with polystyrene homopolymer (PS) [17]. The L_4 phase, which is stable for PSEBS volume fractions (ϕ) less than about 0.2, consists of ethylene-butylene-rich membranes about 19 nm thick. There are important differences between the equilibrium vesicles found for PSEBS in PS and the microemulsion droplets studied earlier [5,6,10,11,13]. First, because the PSEBS membranes are built out of long-chain polymers rather than small-molecule amphiphiles, we may anticipate that features associated with the polymeric character of their constituents could be important in determining the PSEBS vesicles' dynamical behavior, such as a viscoelastic response [4,18–20]. Second, in the case of PSEBS membranes, because the partition coefficient of the short-chain PS homopolymer is significant within all three blocks of the copolymer, permitting a significant membrane permeability, it seems possible that there could be appreciable fluid transport across the membrane [7].

One means to characterize the dynamics of membrane fluctuations in PSEBS-PS blends is via measurements of the ISF. But what sort of scattering? The wave vectors necessary to investigate the behavior of individual membranes are too large to be reached by light scattering. Moreover, these blends are turbid. At the same time, fluctuations of self-assembled polymer-melt microstructures are generally too slow to be accessible in neutron spin echo measurements. Thus, we are led to the emerging technique of x-ray photon correlation spectroscopy (XPCS) [21–26]. In this Letter, we present the first measurements of the equilibrium dynamics of polymer membranes in a polymer blend system. Specifically, our measurements yield the ISF versus q and t at several temperatures in a physical system that is very different from those studied previously.

To examine the behavior, as far as possible uncomplicated by interactions among vesicles, while maintaining sufficient scattering intensity, we chose to study a blend with $\phi = 0.03$. The PSEBS [27] used in the present study had $M_w = 83.6$ kg/mole and $M_w/M_n = 1.07$, while the PS homopolymer [28] had $M_w = 4.82$ kg/mole and $M_w/M_n = 1.11$. These materials were codissolved in toluene, filtered to 0.02 μm, and precipitated into cold isopropanol. The resultant blend was then annealed under vacuum at 160 °C for at least a week prior to the x-ray measurements, which were performed at beam line 8-ID at the Advanced Photon Source (APS). Small-angle x-ray scattering (SAXS) measurements confirm that the sample shows a membrane microstructure, consistent with Ref. [17]. The solid circles in Fig. 1 show the SAXS intensity

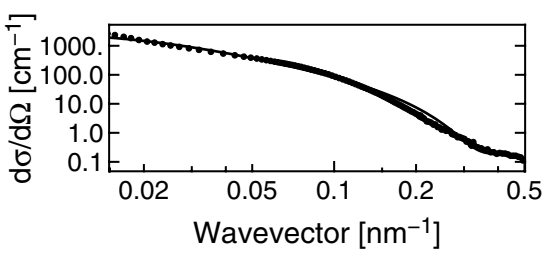

FIG. 1. X-ray scattering cross section ($d\sigma/d\Omega$) for $\phi = 0.03$ PSEBS vs wave vector (solid circles) at 180 °C. The solid line is the model described in the text.

versus wave vector (q) for the sample studied here, while the line corresponds to a Lorentzian profile with a best-fit half-width-at-half-maximum (HWHM) of 0.02 nm^{-1}, multiplied by the form factor of membranes 19 ± 0.6 nm in thickness. We chose a Lorentzian, first, because it provides a good description of the SAXS data throughout the q range studied using few parameters. In addition, the q^{-2} behavior of a Lorentzian for qs greater than the HWHM mimics the scattering intensity expected for membranes. We may therefore ascribe the intensity observed for $q \gtrsim 0.03$ nm^{-1} to individual membranes.

The methodology for XPCS experiments at 8-ID is described elsewhere [29]. In brief, the sample's dynamical properties are characterized via intensity autocorrelation of sequential two-dimensional scattering patterns, obtained under partially-coherent illumination. At each measurement temperature, we acquired several sequences of 850 time-resolved images of the scattered intensity, using full-frame rates of both 62 Hz and 5 Hz, corresponding to exposure times of 17 ms and 204 ms, respectively. To minimize any possible effects of x-ray sample damage, for each data acquisition sequence, the sample position was adjusted to illuminate a fresh spot on the sample. XPCS measures the normalized intensity-intensity time-autocorrelation function: $g_2(q, t) = \langle I(q, t')I(q, t' + t)\rangle / \langle I(q, t')\rangle^2$, where t is the delay time, $I(q, t')$ is the scattering strength at wave vector q and time t', and the brackets $\langle \cdots \rangle$ refer to averages over time t'. The autocorrelation function is related to the ISF via $g_2(q, t) = 1 + A[f(q, t)]^2$, where A is the speckle contrast. For each image sequence, we calculated g_2 pixel by pixel versus delay time [30]. To achieve an acceptable signal-to-noise ratio, for each temperature, we averaged the pixel g_2s over all pixels within some range of a given wave vector.

Figure 2 plots representative intensity autocorrelation functions so-obtained for 140 °C at four different wave vectors versus delay time on a logarithmic scale. These data extend over four decades in delay time, from a shortest delay time of 17 ms to a longest delay time of 170 s. The signal-to-noise ratio is in all cases sufficient to establish the value of g_2 in the short-time limit. In fact, in addition to obtaining values for the characteristic relaxation rate, these data are of high enough quality to make feasible investigations of the autocorrelation line shapes.

We are unaware of predictions for the ISF of an L_4 phase. However, Frey and Nelson [7] and Zilman and Granek [9,12] calculated the normalized ISF [$f(q, t)$] versus wave vector (q) and time (t) for individual membrane plaquettes, which nevertheless should be applicable to vesicles at sufficiently large wave vectors, At short delay times, Ref. [12] specifically predicts that

$$f(q, t) = \exp[-(\Gamma t)^{\alpha}], \quad (1)$$

where $\alpha \simeq \frac{2}{3}(1 + \nu)$, and

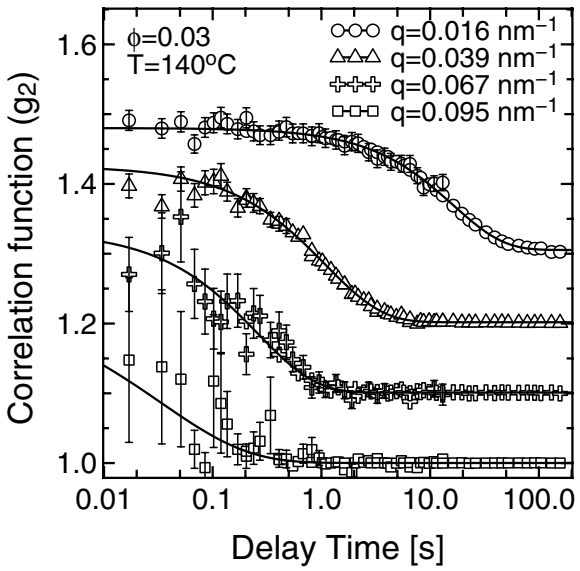

FIG. 2. Intensity autocorrelation functions (g_2) vs delay time at 140 °C for wave vectors of 0.016 nm^{-1} (open circles), 0.039 nm^{-1} (open triangles), 0.067 nm^{-1} (open crosses), and 0.095 nm^{-1} (open squares). The solid lines correspond to least-squares fits to a stretched-exponential form for the ISF. For clarity, the curves have been shifted by 0.1 from each other. Error bars are only shown if they are bigger than the symbols.

$$\Gamma = \left[0.025\left(\frac{12.56\kappa}{\xi^3\eta}\right)^{\nu}\left(\frac{k_BT}{\kappa}\right)^{1/2}\left(\frac{k_BTq^3}{\eta}\right)\right]^{1/(1+\nu)}, \quad (2)$$

with η the fluid viscosity, κ the membrane bending modulus, $\nu \simeq k_BT/4\pi\kappa$, and ξ a long length scale cutoff. Evidently, in the case that $\kappa \simeq k_BT$, the ISF is predicted to show a stretched-exponential behavior versus t with a stretching exponent $\alpha \simeq 2/3$ and a relaxation rate that varies approximately as q^3. Such behavior has also been observed experimentally in other membrane-based phases, including in highly swollen L_α and L_3 phases, which were studied via dynamic light scattering [31], and in bicontinuous microemulsion phases, which were studied using the neutron spin echo technique under film contrast conditions [32].

Inspired by these predictions, we fit the g_2s to the form expected for a stretched-exponential ISF [Eq. (1)]. The resultant best-fit model g_2s, which are shown as the solid lines in Fig. 2, provide an excellent description of the experimental data. To clarify the extent to which these data require a stretched-exponential ISF rather than a strictly exponential form, in Fig. 3 we present ISFs [$f(q, t) = \sqrt{(g_2 - 1)/A}$] obtained at 160 °C, plotted as the open symbols versus reduced-delay time, Γt, where t is the delay time and Γ is the best-fit relaxation rate for the data in question. This plot extends to $\Gamma t = 2$, thus focusing on the short-time limit, which is where the stretched-exponential prediction is applicable [12]. The solid lines

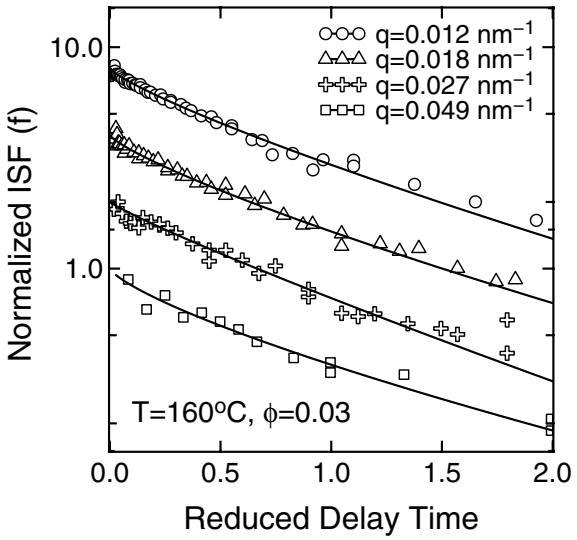

FIG. 3. Normalized intermediate scattering functions (f) plotted vs reduced-delay time (Γt) at 160 °C for wave vectors of 0.012 nm^{-1} (open circles), 0.018 nm^{-1} (open triangles), 0.027 nm^{-1} (open crosses), and 0.049 nm^{-1} (open squares), plotted on a logarithmic intensity scale and a linear reduced-delay time scale. The solid lines are a stretched-exponential form, as discussed in the text. For clarity, data and model have been multiplied 8, 4, 2, 1 for wave vectors of 0.012 nm^{-1}, 0.018 nm^{-1}, 0.027 nm^{-1}, and 0.049 nm^{-1}, respectively.

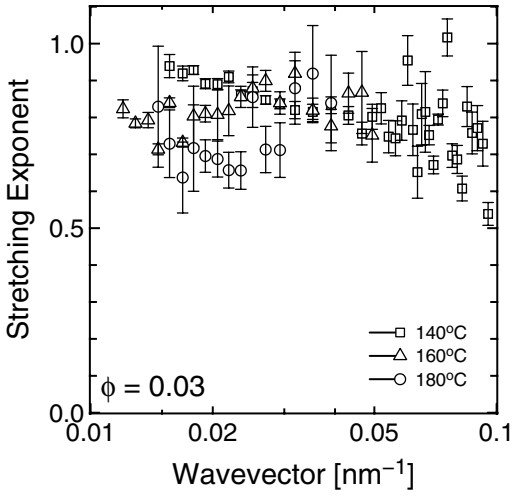

FIG. 4. Stretching exponents for the $\phi = 0.03$ sample, for 180 °C (open squares), 160 °C (open crosses), and 140 °C (open triangles).

in Fig. 3 are the ISFs corresponding to the best-fit model g_2s. The logarithmic intensity scale and linear time scale of this figure imply that an exponential ISF (i.e., $\alpha = 1$) would appear as a straight line. By contrast, the measured ISFs clearly exhibit a small curvature, demonstrating a deviation from single-exponential relaxation. Although Figs. 2 and 3 make it clear that the stretched-exponential model provides an excellent account of the measured g_2s, we have not established the uniqueness of this particular description.

Stretched-exponential fits were carried out for data obtained at each temperature studied and for each wave number partition. The best-fit stretching exponents are shown in Fig. 4 for 180 °C (circles), 160 °C (triangles), and 140 °C (squares). Evidently, the stretching exponent is only weakly dependent on wave vector and temperature with a value of about $\alpha \simeq 0.8 \pm 0.1$. A stretched-exponential ISF with a stretching exponent that is slightly larger than $\alpha = 2/3$ is consistent with the prediction of Ref. [12] [Eq. (1)], where a stretching exponent in the range between 0.7 and 0.9 would correspond to a value for κ between 1.7 and $0.23 k_B T$.

The corresponding best-fit relaxation rates increase rapidly and monotonically with increasing wave vector (q) in a more or less power-law fashion, with similar exponents at each temperature. In addition, they show a strong temperature dependence, with significantly faster relaxations at higher temperatures. Because the PS homopolymer viscosity decreases by a factor of about 40 as the temperature is increased from 140 °C ($\eta \simeq 240$ Poise) to 180 °C ($\eta \simeq 6$ Poise) [33,34], according to Eq. (2), we should expect the temperature dependence of the relaxation rate to be dominated by the PS viscosity. For $\kappa \simeq k_B T$, ν is small, and it is sensible to approximate $\nu \simeq 0$. In this case, the relaxation rate (Γ) is predicted to vary nearly linearly versus $k_B T q^3/\eta$. How the experimental relaxation rate actually depends on $k_B T q^3/\eta$ is shown in Fig. 5 for 180 °C

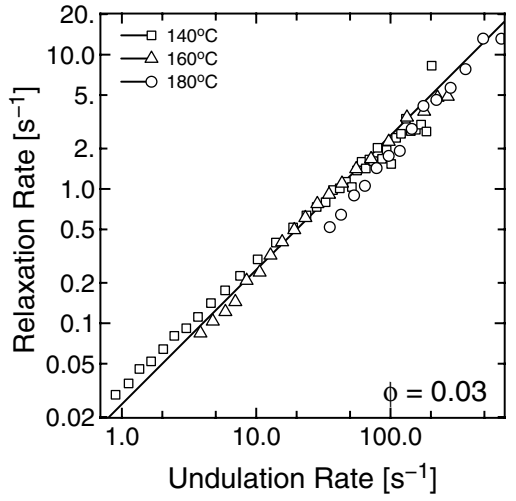

FIG. 5. Fitted relaxation rates (Γ) plotted versus the undulation rate, defined as $k_B T q^3/\eta$, for 180 °C (circles), 160 °C (triangles), and 140 °C (squares), determined from stretched-exponential fits of the sort illustrated in Fig. 2. The solid line corresponds to the prediction of Refs. [9,12] for $\nu = 0$, namely $\Gamma = 0.025 \kappa q^3/\eta$.

(circles), 160 °C (triangles), and 140 °C (squares). Evidently, the observed behavior is approximately consistent with the prediction. Beyond its q and T dependence, we may also compare the absolute value of the relaxation rate to theory. For $\nu \simeq 0$, Ref. [12] predicts that $\Gamma \simeq 0.025 k_B T q^3/\eta$. This is shown as the solid line in the figure, showing overall good agreement with the data.

It is initially surprising that the agreement appears so satisfactory, in part, because of the differences, noted above, between the polymeric membranes, studied here, and the idealized membranes of the theory, but also because the qs probed in this experiment—from 0.015 nm^{-1} to 0.1 nm^{-1}—are comparable to the HWHM of the SAXS profile (0.02 nm^{-1}), suggesting that interactions between membranes become significant for $q \lesssim 0.02$ nm^{-1}. For qs increasing above 0.02 nm^{-1}, however, the SAXS intensity converges rapidly to that expected for individual membranes. In this regime, therefore, the theory should be applicable. The fact that the behavior for smaller qs is also consistent with theory suggests that in this regime, too, we are examining the dynamics of individual membranes. However, we cannot rule out other, unexplored mechanisms that coincidentally mimic the predicted behavior. In this regard, we note that a relaxation rate proportional to $k_B T q^3/\eta$ follows on dimensional grounds in the absence of a characteristic length scale.

In detail, examination of Fig. 5 reveals that the data obtained at the different temperatures do not collapse perfectly to a single curve. This behavior might be associated with the small systematic variation of the best-fit stretching exponent for different temperatures, which may be discerned in Fig. 4. Overall, however, our data are well described by the theories of Refs. [7,9,12], which treat the dynamics of independent membrane plaquettes. The points of agreement include: stretched-exponential behavior of the ISF with a stretching exponent near 2/3 and a relaxation rate that shows an approximate q^3 dependence on wave vector and is inversely proportional to the homopolymer viscosity. In addition, the absolute value of the relaxation rate lies close to what is predicted. Beyond providing support for the description of membrane dynamics given in Refs. [7,9,12], the larger significance of these results is that they bolster the notion that membrane undulations can play a key role in determining the behavior within high polymer systems, as indicated in Ref. [35], just as they do in membrane-based materials containing small-molecule amphiphiles, where such fluctuations are central to our present understanding [36].

We thank D. Lumma, L. Lurio, S. Narayanan, and A. Sandy for valuable discussions, and H. Gibson for technical assistance. This research was supported by the NSF via DMR 0071755. The APS is supported by DOE BES.

[1] M. B. Schneider, J. T. Jenkins, and W. W. Webb, J. Phys. (France) **45**, 1457 (1984).
[2] H. Engelhardt, H. P. Duwe, and E. Sackmann, J. Phys. Lett. **46**, L395 (1985).
[3] B. Discher *et al.*, Science **284**, 1143 (1999).
[4] R. Dimova *et al.*, Eur. Phys. J. E **7**, 241 (2002).
[5] J. S. Huang *et al.*, Phys. Rev. Lett. **59**, 2600 (1987).
[6] B. Farago *et al.*, Phys. Rev. Lett. **65**, 3348 (1990).
[7] E. Frey and D. R. Nelson, J. Phys. I (France) **1**, 1715 (1991).
[8] S. Komura and K. Seki, Physica A (Amsterdam) **192**, 27 (1993).
[9] A. G. Zilman and R. Granek, Phys. Rev. Lett. **77**, 4788 (1996).
[10] T. Hellweg *et al.*, Colloids Surf. A **183-185**, 159 (2001).
[11] B. Farago and M. Gradzielski, J. Chem. Phys. **114**, 10105 (2001).
[12] A. G. Zilman and R. Granek, Chem. Phys. **284**, 195 (2002).
[13] Y. Kawabata *et al.*, Phys. Rev. Lett. **92**, 056103 (2004).
[14] S. T. Milner and S. A. Safran, Phys. Rev. A **36**, 4371 (1987).
[15] L. Miao, M. A. Lomholt, and J. Kleis, Eur. Phys. J. E **9**, 143 (2002).
[16] J. H. Laurer *et al.*, Macromolecules **31**, 4975 (1998).
[17] P. Falus *et al.*, Phys. Rev. Lett. **93**, 145701 (2004).
[18] U. Seifert and S. A. Langer, Europhys. Lett. **23**, 71 (1993).
[19] A. Yeung and E. Evans, J. Phys. II (France) **5**, 1501 (1995).
[20] E. Helfer *et al.*, Phys. Rev. Lett. **85**, 457 (2000).
[21] S. G. J. Mochrie *et al.*, Phys. Rev. Lett. **78**, 1275 (1997).
[22] A. C. Price *et al.*, Phys. Rev. Lett. **82**, 755 (1999).
[23] I. Sikharulidze *et al.*, Phys. Rev. Lett. **88**, 115503 (2002).
[24] E. M. Dufresne, T. Nurushev, R. Clarke, and S. B. Dierker, Phys. Rev. E **65**, 061507 (2002).
[25] H. J. Kim *et al.*, Phys. Rev. Lett. **90**, 068302 (2003).
[26] A. Madsen *et al.*, Phys. Rev. Lett. **92**, 96104 (2004).
[27] Shell International, Houston, TX.
[28] Polymer Source, Inc., Dorval, QC, Canada.
[29] P. Falus, M. Borthwick, and S. G. J. Mochrie, Rev. Sci. Instrum. **75**, 4383 (2004).
[30] "Coherent" software package, available for download from http://xpcs.physics.yale.edu/coherent/.
[31] E. Freyssingeas and D. Roux, J. Phys. II (France) **7**, 913 (1997).
[32] M. Mihailescu *et al.*, J. Chem. Phys. **115**, 9563 (2001).
[33] D. J. Plazek and V. M. O'Rourke, J. Polym. Sci., A-2, Polym. Phys. **9**, 209 (1971).
[34] T. G. Fox and P. J. Flory, J. Appl. Phys. **21**, 581 (1950).
[35] P. Stepanek *et al.*, Macromolecules **35**, 7287 (2002).
[36] C. R. Safinya *et al.*, Phys. Rev. Lett. **57**, 2718 (1986).